Iraqi Journal of Physics, 2023 *Vol. 21 No. 4, PP. 92-102*
https://doi.org/10.30723/ijp.v21i4.1138 *P-ISSN: 2070-4003*
E-ISSN: 2664-5548

Characterization and Photovoltaic Effect of (Sb_2O_3: Metal Oxides)/ c-Si Heterojunctions

Mohammed I. Tareq[1a*] and Bushra A. Hasan[1b]
[1]*Department of Physics, College of Science, University of Baghdad, Baghdad, Iraq*
[b]E-mail: bushra_abhasan@yahoo.com
[a*]Corresponding author: mohammed.imad.tareq@gmail.com

Abstract

This work concerns the synthesis of two types of composites based on antimony oxide named (Sb_2O_3):(WO_3, In_2O_3). Thin films were fabricated using pulsed laser deposition. The compositional analysis was explored using Fourier transform infrared spectrum (FTIR), which confirms the existence of antimony, tungsten, and indium oxides in the prepared samples. The hall effect measurement showed that antimony oxide nanostructure thin films are p-type and gradually converted to n-type by the addition of tungsten oxide, while they are converted almost instantly to n-type by the addition of indium oxide. Different heterojunction solar cells were prepared from (Sb_2O_3:WO_3, In_2O_3/Sb_2Se_3/c-pSi) contained forms from two layers the first was Sb_2Se_3 and the second was (Sb_2O_3):(WO_3, In_2O_3) nanostructured thin films. The heterojunction (Sb_2O_3:15%WO_3 Sb_2Se_3/c-pSi showed a maximum conversion efficiency of 9% and exhibits an open circuit voltage (V_{oc}) of 300 mV, short circuit current (I_{sc}) of 35 mA, and a fill factor of 0.429 at an intensity of illumination of 100 mW/cm^2.

Article Info.

Keywords:
Solar Cell, Pulsed Laser Deposition, Sb_2O_3 Thin Films, FTIR Spectrum, Hall Effect.

Article history:
Received: Jun. 06, 2023
Revised: Sep. 12, 2023
Accepted: Sep. 24, 2023
Published: Dec. 01,2023

1. Introduction

Antimony trioxide (Sb_2O_3) stands out among V-VI semiconductors due to its broad and direct band gap in the near ultraviolet region [1-3]. According to "handbook-data", the melting point of antimony trioxide is 655°C and the effervescence point is 1550°C, and vapor compression at ambient temperature is believed to be relatively minimal [4, 5]. Numerous researches have looked at the various methods for preparing and characterizing thin films of V-VI group compounds [6, 7]. This material's thin films have numerous desirable optical properties, such as high transmittance at visible and infrared wavelengths and high absorption in the ultraviolet region [1, 8]. One of the semiconductors in this family is antimony trioxide (Sb_2O_3). Because of its structural, optical, electrical, and photoelectronic capabilities, it is a material of relevance in the fields of both fundamental research and technical applications. The design and development of thin-film devices like low-loss high-reflecting mirrors used for various high-power laser and interferometric applications in the ultraviolet and visible region requires information on the optical constants of thin semiconductor films, specifically their refractive index n, their absorption coefficient, and their optical band gap E_g [9, 10]. Thin semiconductor Sb_2O_3 films have many applications, including laser visible diodes, coatings, solar cells, infrared detectors, ultraviolet filters, and more, so it is important to have information on their optical constants, such as their transmittance, absorbance, and optical band gap, E_g [4, 11].

As a result of their great sensitivity to low gas concentrations, Sb_2O_3 thin films have gained a lot of attention in recent years for use in critical sensor materials for detecting leakage of dangerous gases. gas sensors and solar cells [12, 13]. This research aims to study the composition of composite nanofilms prepared from antimony oxide: tungsten oxide and antimony oxide: indium oxide using Fourier transform infrared

spectrum (FTIR), and then study the type of these thin films by measuring the hall effect, and finally prepared heterojunctions and measuring current-voltage in the dark and the light.

2. Experimental Work

The composition analysis of the antimony trioxide unmixed and mixed with WO_3 and In_2O_3 thin films was determined (FTIR 8400s) the spectra of Sb_2O_3 and Sb_2O_3:WO_3, In_2O_3 thin films were recorded in the range 400-4000 cm^{-1}. The fabrication process for the heterojunction solar cells was consistent; Sb_2Se_3 was deposited to increase cell efficiency, and a thin layer (Sb_2O_3:WO_3, In_2O_3) was deposited using the pulsed laser deposition method on single crystal silicon p type. Samples that were prepared were subjected to I-V measurement in the dark and under illumination.
From the plots of the relation between bias voltage and forward current, the factor of ideality (β) [14] could be specified as follows:

$$I = I_o \exp qV\beta / kBT \quad (\mathbf{1})$$

and the equation of Fill factor (F.F) is given by:

$$F.F = V_m \frac{I_m}{V_{oc}} I_{oc} \quad (\mathbf{2})$$

The photovoltaic conversion efficiency (PCE) can be characterized as:

$$\eta = \frac{P_m}{P_{in}} = \frac{F.F_x I_{scx} V_{oc}}{P_{in} x100} \% \quad (\mathbf{3})$$

The preparation of (Sb_2O_3) unmixed and mixed with different ratios of WO_3 and In_2O_3 compounds and thin films using the pulsed laser deposition method on various substrates like glass for FTIR analysis, Hall effect measurement and, single crystal Silicon wafers c-Si (p–type). The Si single crystal wafers p-type substrates with the orientation of the crystal (100), (1.50-5 Ω.cm) range of the electrical resistivity, $1.45x10^{10} cm^{-3}$ carriers' concentration, the minimal indirect energy gap of 1.10 eV have been cleaned with the use of the etching process, which can be summarized as: silicon wafers have been immersed and stirred in a chemical solution that consists of 3 ml HNO_3 and 1 ml HF for (1–3min). Then they were rinsed with the distilled water for several times. Finally, silicon wafers have been dried with the use of soft paper.

Sb_2O_3:WO_3, In_2O_3 compounds were prepared by heating the amounts of matrix oxide with the dopant oxide according to the demand ratios at a temperature of 1273 K for five hours, then they were left to slowly cool to the temperature of the room.

Fig. 1 illustrates the structure of the prepared heterojunction solar cell in this study. The device structure comprises, from bottom to top, a layer of aluminum acting as the back contact (approximately 200nm thick), followed by single crystal wafers of p-type silicon, a Sb_2Se_3 layer (t=300±10 nm), and a final layer of Sb_2O_3:WO_3 and In_2O_3 deposited to a thickness of 150nm. The wires were connected using silver paste. Current-voltage measurements in the dark have been carried out for Sb_2O_3:WO_3, In_2O_3 /p-Si, heterojunctions with the use of the Keithley digital electro-meter 616 and DC power supply. The bias voltage has been varied in a range between (-1V to 1V) in the case of the reverse and forward bias. I-V illumination measurements were made for prepared cells by exposing them to a Halogen lamp light Philips (120 W) and 100 mW/cm^2 intensity. The sun-light incident on the device from the top can be seen in Fig. 1.

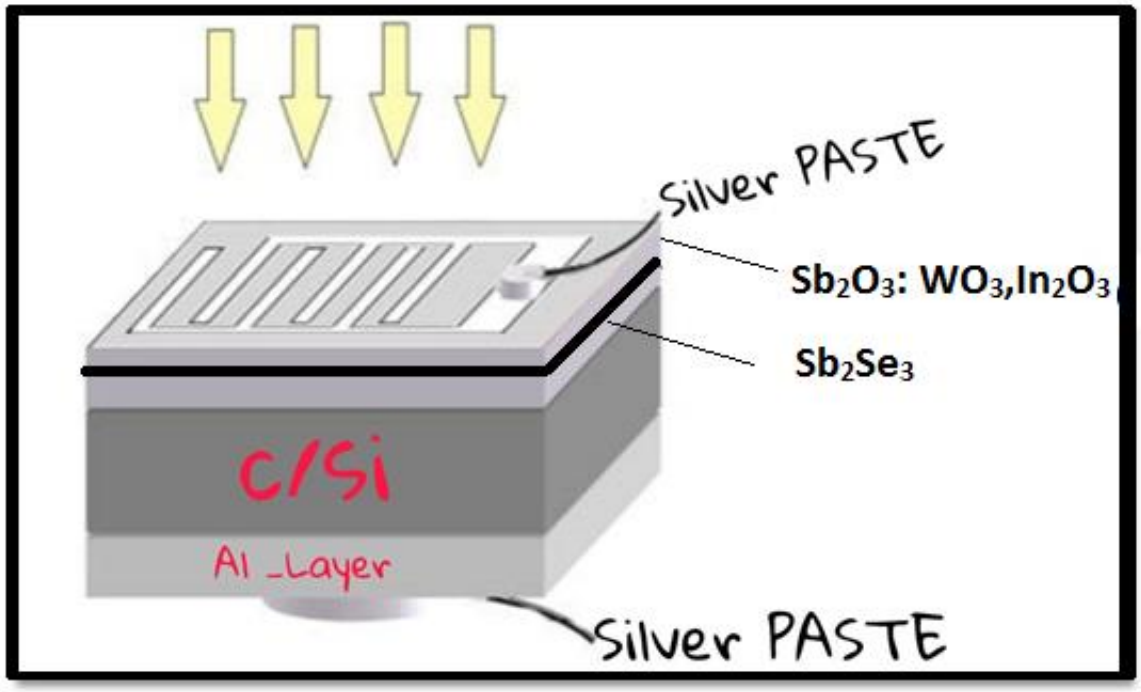

Figure 1: Structure of Sb_2O_3:WO_3, In_2O_3/p-Si solar cell.

3. Results and Discussion

3.1. Structural Analyses of (Sb_2O_3):(WO_3,In_2O_3) Thin Films

The FTIR spectra of Sb_2O_3 and (Sb_2O_3:WO_3, In_2O_3) have been recorded in a range of 400-4000cm^{-1} at Pure Sb_2O_3 The specific peaks were identified and matched with the standard values done by previous researches. Fig. 2 shows the FTIR spectra of Sb_2O_3 thin films with 0.0% of the mixing concentration. Because of the absorption peak values of Sb–O–Sb, Sb–O, and Sb–OH bond vibrations, the bands were allocated. The presence of OH on the adsorbed water and Sb–OH causes the strong absorption band at 3787.21cm^{-1} and the band at 3435.01cm^{-1}. The peaks at 741.06 cm^{-1} are assigned to the Sb–O–Sb vibrations [15-17]. The strong band at 2354 cm^{-1} is due to CO_2 stretching vibration according to Ref. [18, 19].

FTIR of synthesized Sb_2O_3 mixed WO_3 of the concentrations (0.05,0.10, and 0.15) is shown in Figs. 3, 4, and 5. The W–O and W–O–W vibrations of WO_3 are ascribed to the peaks at 614.22 and 610 cm^{-1} [20, 21]. The infrared absorption becomes stronger as the mixing concentration increases, indicating that the W–O and W–O–W content have risen. It means that as the temperature of the annealing was raised, oxygen vacancies were filled with oxygen elements, resulting in W–O and W–O–W bonds. The FTIR of the synthesized Sb_2O_3 mixed In_2O_3 of the concentrations (0.05,0.10, and 0.15) is shown in Figs. 6, 7, and 8. Two peaks centered at 617, and 470 cm^{-1} were observed, which are characteristic of the In-O and In-O-In stretching respectively [22-24].

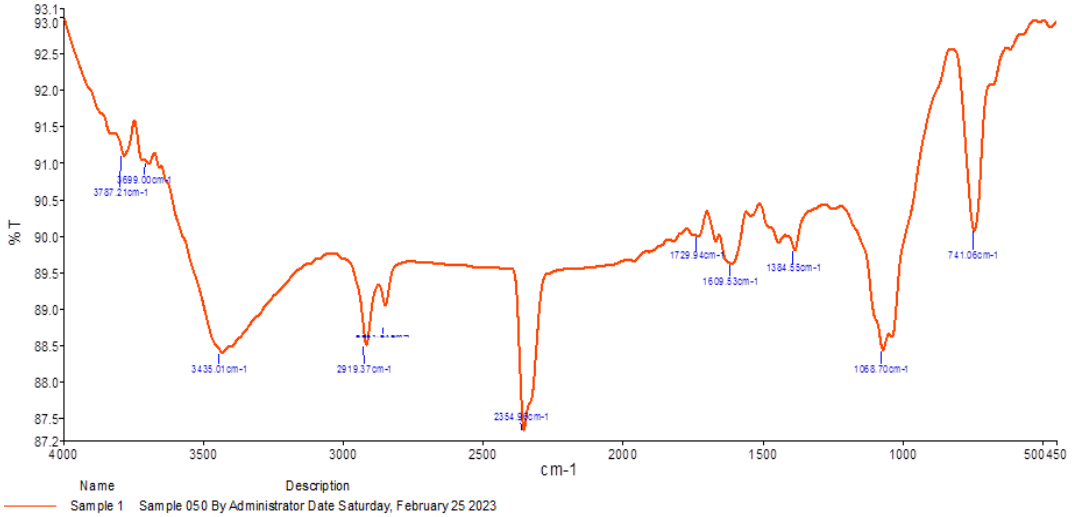

Figure 2: FTIR spectrum of Sb_2O_3 thin films.

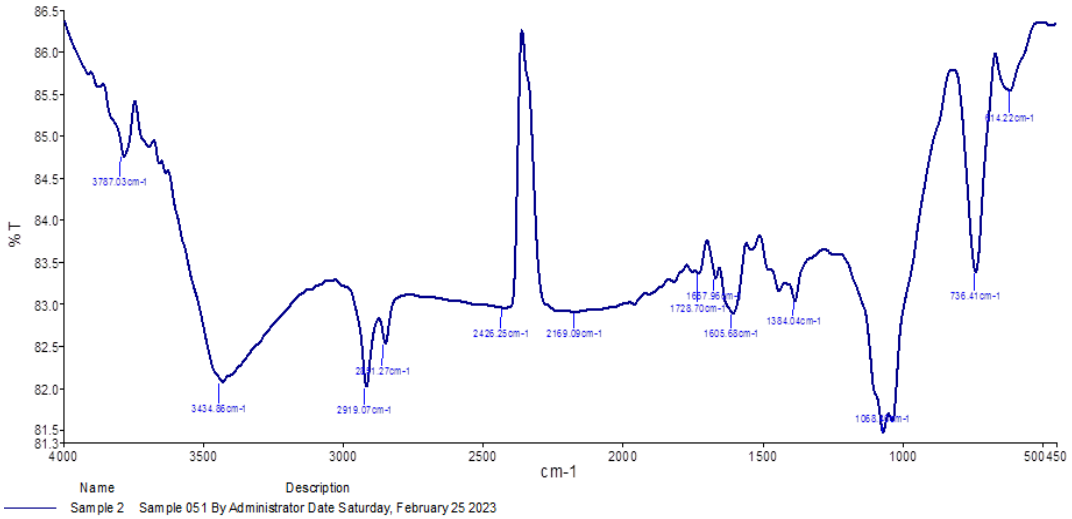

Figure 3: FTIR spectrum of Sb_2O_3:5%WO_3 thin films.

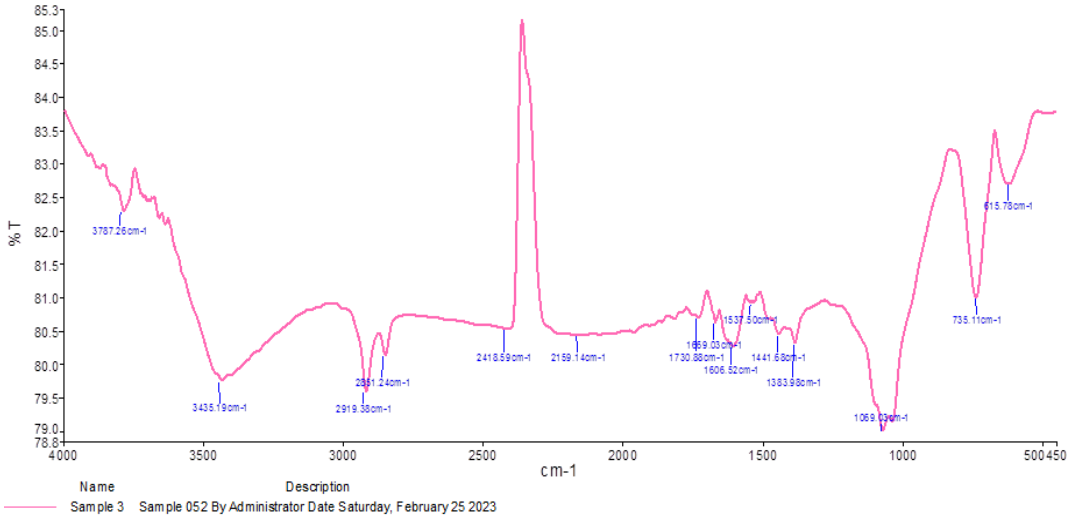

Figure 4: FTIR spectrum of Sb_2O_3:10%WO_3 thin films.

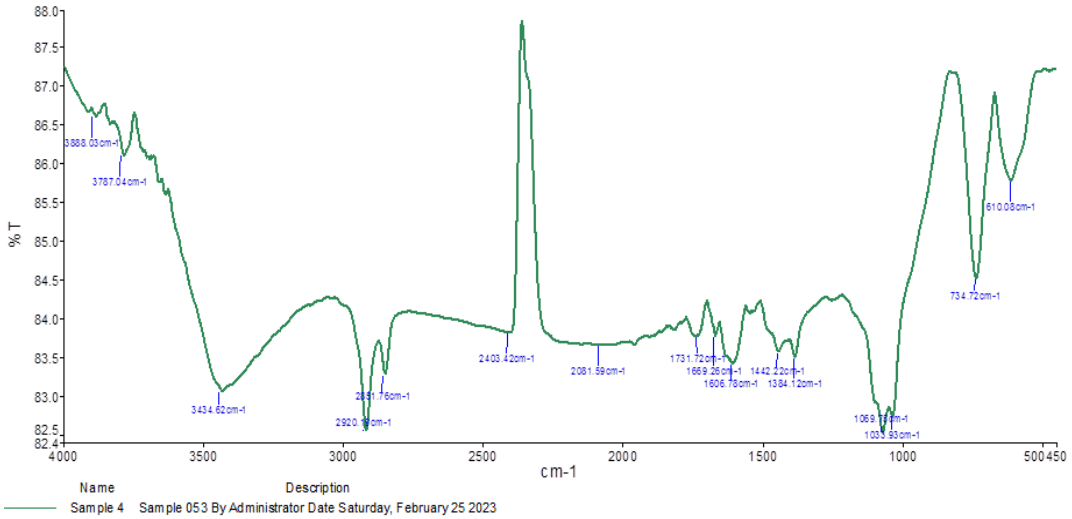

Figure 5: FTIR spectrum of Sb_2O_3: 15%WO_3 thin films.

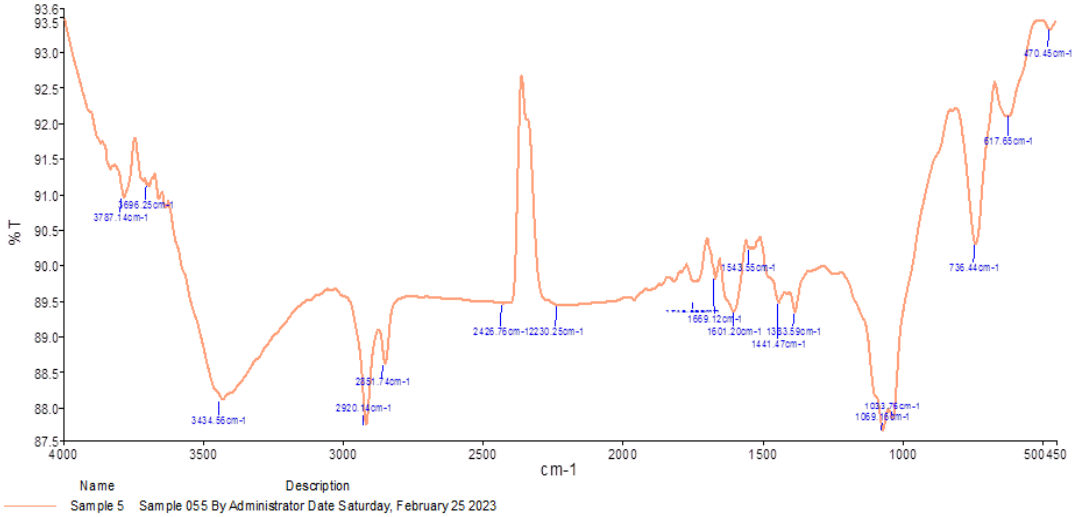

Figure 6: FTIR spectrum of Sb_2O_3:5% In_2O_3 thin films.

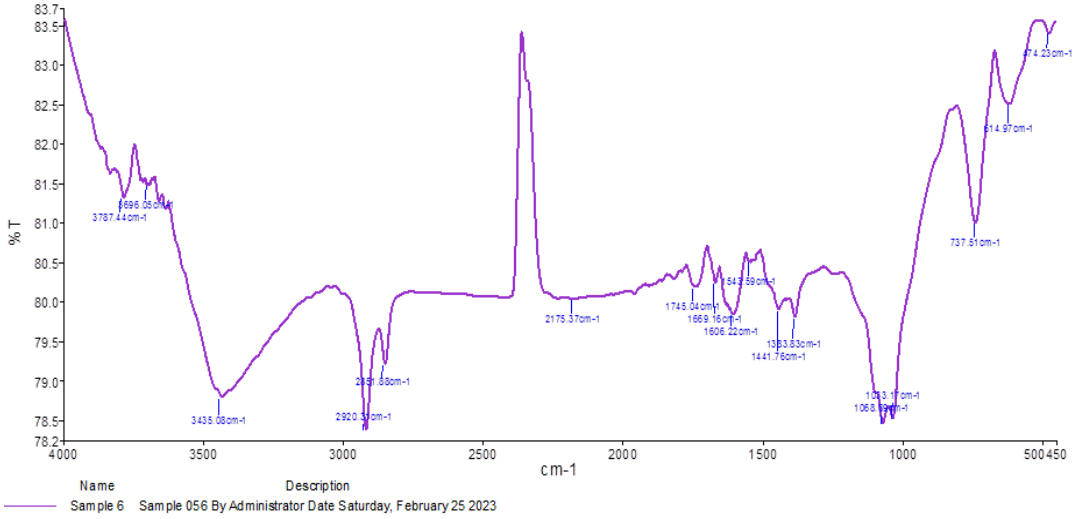

Figure 7: FTIR spectrum of Sb_2O_3:10% In_2O_3 thin films.

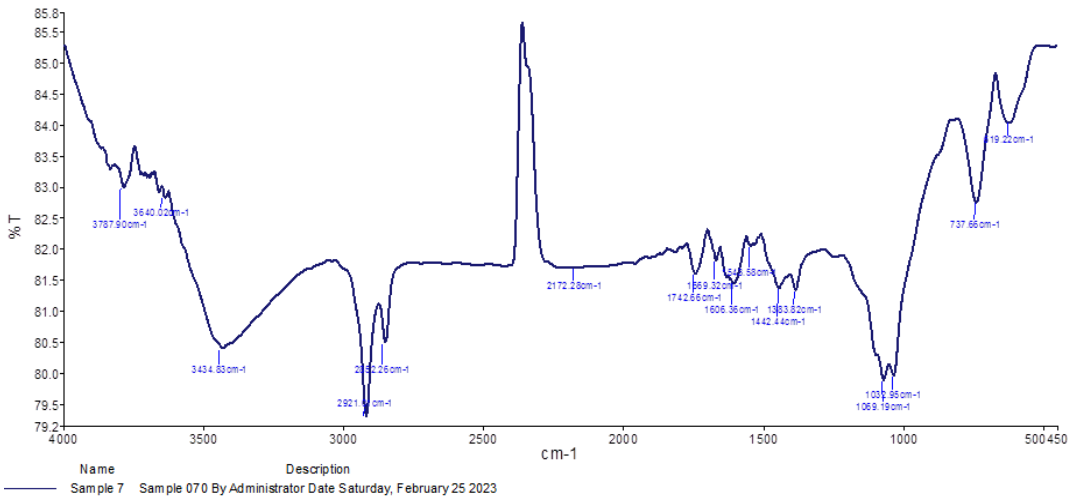

Figure 8: FTIR spectrum of Sb_2O_3:15%In_2O_3 thin films.

3.2. Electrical Properties

3.2.1. Hall Effect Measurement

Hall measurements were conducted to estimate the charge carrier type, carrier concentration (n_H), and Hall mobility (μ_H) of the charge carriers. Hall measurements of all the prepared thin films from (Sb_2O_3):(WO_3, In_2O_3) films deposited on the glass substrate are listed in Table (1). It was evident from this table that most of the thin film samples revealed a negative Hall coefficient (n-type charge carriers), that is, the Hall voltage decreased with increasing current, except the samples pure Sb_2O_3 and Sb_2O_3: 5%WO_3 which have positive Hall coefficient (p-type), i.e., the hall voltage increased with increasing the current [25-28]. The concentration of the carrier n_H of the prepared thin films (Sb_2O_3:WO_3) decreased in a non-regular manner with the increasing of the WO_3 content, i.e., to reduce by addition of WO_3 while it was found to grow up by increasing of In_2O_3 to the starting material. While μ_H Hall mobility changed oppositely to that. The addition of (WO_3, In_2O_3) has an important role in carrier concentration and mobility. The maximum accumulated conductivity of (Sb_2O_3:WO_3) thin films at the mixing ratio of 5% was 1.75×10^2 ($\Omega^{-1}.cm^{-1}$) and of (Sb_2O_3: In_2O_3) films at the mixing ratio 15% was 1.64×10^2 ($\Omega^{-1}.cm^{-1}$) while the lowest conductivity for (Sb_2O_3:WO_3)films was 7.04×10^0($\Omega^{-1}.cm^{-1}$) occurred at 15% and 1.13×10^2 ($\Omega^{-1}.cm^{-1}$) for (Sb_2O_3: In_2O_3) films at the ratio 10% as can be observed from Table(1) which showed the values of charge concentration (n_H), Hall mobility (μ_H) and the type of charge carriers for (Sb_2O_3):(WO_3, In_2O_3) thin films prepared with PLD technique.

Table 1: Hall effect parameters for (Sb_2O_3):(WO_3, In_2O_3) thin film.

Sample	μ_H ($cm^2/V.s$)	R_H (m^2/C)	n_H (cm^{-3})	$\sigma_{R.T}$ ($\Omega^{-1}.cm^{-1}$)	type
Sb_2O_3	1.54×10^5	5.57×10^2	1.12×10^{16}	2.76×10^2	p
Sb_2O_3:5%WO_3	2.27×10^5	5.22×10^3	1.19×10^{16}	4.35×10^2	p
Sb_2O_3:10%WO_3	9.69×10^3	-6.62×10^2	-9.42×10^{16}	1.46×10^1	n
Sb_2O_3:15%WO_3	3.80×10^4	-2.44×10^3	-2.65×10^{16}	1.56×10^2	n
Sb_2O_3: 5%In_2O_3	7.43×10^4	-4.95×10^2	-1.26×10^{16}	1.50×10^2	n
Sb_2O_3:10% In_2O_3	1.57×10^4	-1.39×10^2	-4.49×10^{16}	1.13×10^2	n
Sb_2O_3:15% In_2O_3	1.15×10^4	-7.00×10^1	-8.92×10^{16}	1.64×10^2	n

3.2.2. Current–Voltage Characteristics of (Sb_2O_3:WO_3, In_2O_3/Sb_2Se_3/c-pSi) Heterojunctions

A photodiode and a solar cell have many similarities. By being biased and coupled to a load impedance, the photodiode can be used in a photovoltaic application. The devices function similarly, yet their designs are very different. However, solar cells need to have a wide spectrum response over a broad solar wavelength range, but photodiodes only care about a restricted wavelength range centered at the optical signal wavelength. While solar cells have a huge surface area, photodiodes are typically quite tiny to reduce junction capacitance. In contrast to solar cells, which are primarily concerned with power conversion efficiency (power delivered to the load per incident solar energy), photodiodes place a premium on quantum efficiency [29-34].

A solar cell's composition is split between two "active layers."

1) The thin top layer, also known as the emitter or window layer, is strongly doped.
2) An oppositely doped, thick, bottom layer (the base or absorber) [35-38].

Figs. 9 and 10 show the current-voltage relation in the dark condition of the prepared heterojunctions. It is clear that they operate as rectifiers i.e., pass current in forward biasing and very low current passes in reverses biasing on the other hand the dark current of the WO_3 mixed Sb_2O_3/Sb_2Se_3/c-Si is lower than that of the In_2O_3 mixed Sb_2O_3/Sb_2Se_3/c-Si heterojunctions [39-41].

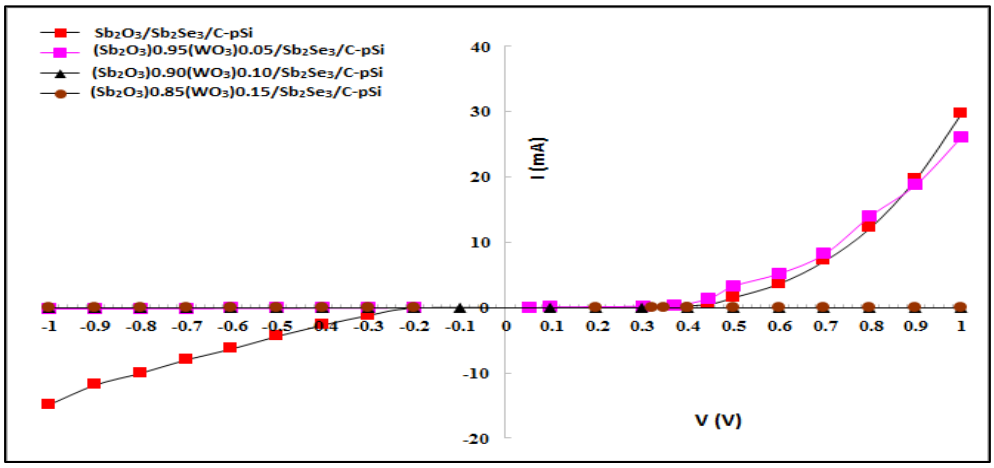

Figure 9: Current versus applied voltage in the dark of (Sb_2O_3:WO_3 /Sb_2Se_3/c-pSi) heterojunctions.

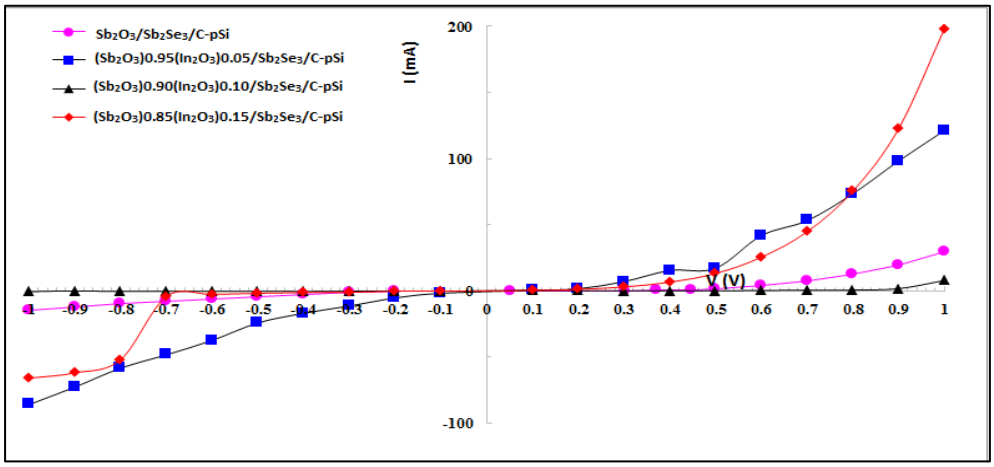

Figure 10: Current versus applied voltage in the dark of (Sb_2O_3:In_2O_3 /Sb_2Se_3/c-pSi) heterojunctions.

Fig. 11 showed I-V characteristics for Sb_2O_3:WO_3, In_2O_3/Sb_2Se_3/c-pSi devices with various compositional ratios under an illumination intensity of 100 mW/cm^2. The corresponding values of V_{oc}, I_{oc}, FF, and conversion efficiency for these heterojunctions are summarized in Table 2. The conversion efficiency of the pristine device without conversion efficiency was 0.16% with V_{oc} of 0.35 V, and I_{sc} of 0.16 mA, and F.F of 92.6%. The increase in WO_3 content reduces the values V_{oc}, I_{sc}, and conversion efficiency. The continuous addition of WO_3 led to increases in the conversion efficiency rapidly to 9% with a significant increase in the values of V_{oc}, I_{sc} this is accompanied by a reduction of the value of the filling factor (inverse relation between filling factor and conversion efficiency). While increasing of compositional ratio of In_2O_3 improved the values of solar cell parameters conversion efficiency, V_{oc}, and I_{sc} in the first stage of addition, the continuous increase of In_2O_3 ratio worsened the performance of the solar throughout reducing the values of conversion efficiency, V_{oc}, and I_{sc}. The increase of the WO_3 ratio which induced performance improvement can be generally attributed to enhanced exciton dissociation at the donor/acceptor interface. The addition of WO_3 may strengthen the donor-acceptor molecular interaction, and thereby boost the carrier exchange process, consequently, the charge separation becomes more efficient. The obtained relatively high conversion efficiency (9%) for Sb_2O_3:15% WO_3/ Sb_2Se_3/c-pSi heterojunction may be attributed to relatively large crystal size (24 nm) and good roughness and enhancement of matching between the absorber and widow layer concluded from ideality factor value in ideal range (1.25) as well as the red shift of band gap since the energy gap reduced from 3.3 to 2.7 eV by the effect of increasing WO_3 from 0 to 0.15. The conversion efficiency depends upon the transport of charge carriers and collection. The absence of a recombination center plays the main role in solar cell performance. The low dark current indicates a low dark current of Sb_2O_3:WO_3/Sb_2Se_3/c-pSi heterojunctions which gives rise to improved conversion efficiency of the solar cell [42-50].

Table 2: The values of I_{sc}, I_m, V_{oc}, V_m, F.F, Pm, Efficiency and Ideality factor of Sb_2O_3:WO_3,In_2O_3 /Sb_2Se_3/c-pSi heterojunctions solar cells.

Sample	I_{sc} (mA)	I_m(mA)	V_{oc}(Volt)	V_m(Volt)	F.F	P_m (mW)	Efficiency	ideality factor
Sb_2O_3/Sb_2Se_3/c-pSi	0.25	0.270	0.35	0.30	0.926	0.081	0.16%	14.91
Sb_2O_3: 5%WO_3/Sb_2Se_3/c-pSi	1.00	1.00	0.0055	0.0025	0.455	0.001	0.002%	5.77
Sb_2O_3:10%WO_3/Sb_2Se_3/c-pSi	2.10	1.90	0.01	0.09	5.816	0.171	0.34%	2.95
$Sb_2O_3$15%WO_3/Sb_2Se_3/c-pSi	35.00	30.00	0.30	0.15	0.429	4.500	9.00%	1.25
Sb_2O_3: 5%In_2O_3/Sb_2Se_3/c-pSi	4.50	3.90	0.14	0.09	0.557	0.351	0.70%	6.83
Sb_2O_3:10%In_2O_3/ Sb_2Se_3/c-pSi	9.00	7.00	0.12	0.08	0.519	0.560	1.12%	9.67
Sb_2O_3:15%In_2O_3/ Sb_2Se_3/c-pSi	0.60	0.60	0.10	0.06	0.600	0.036	0.07%	8.73

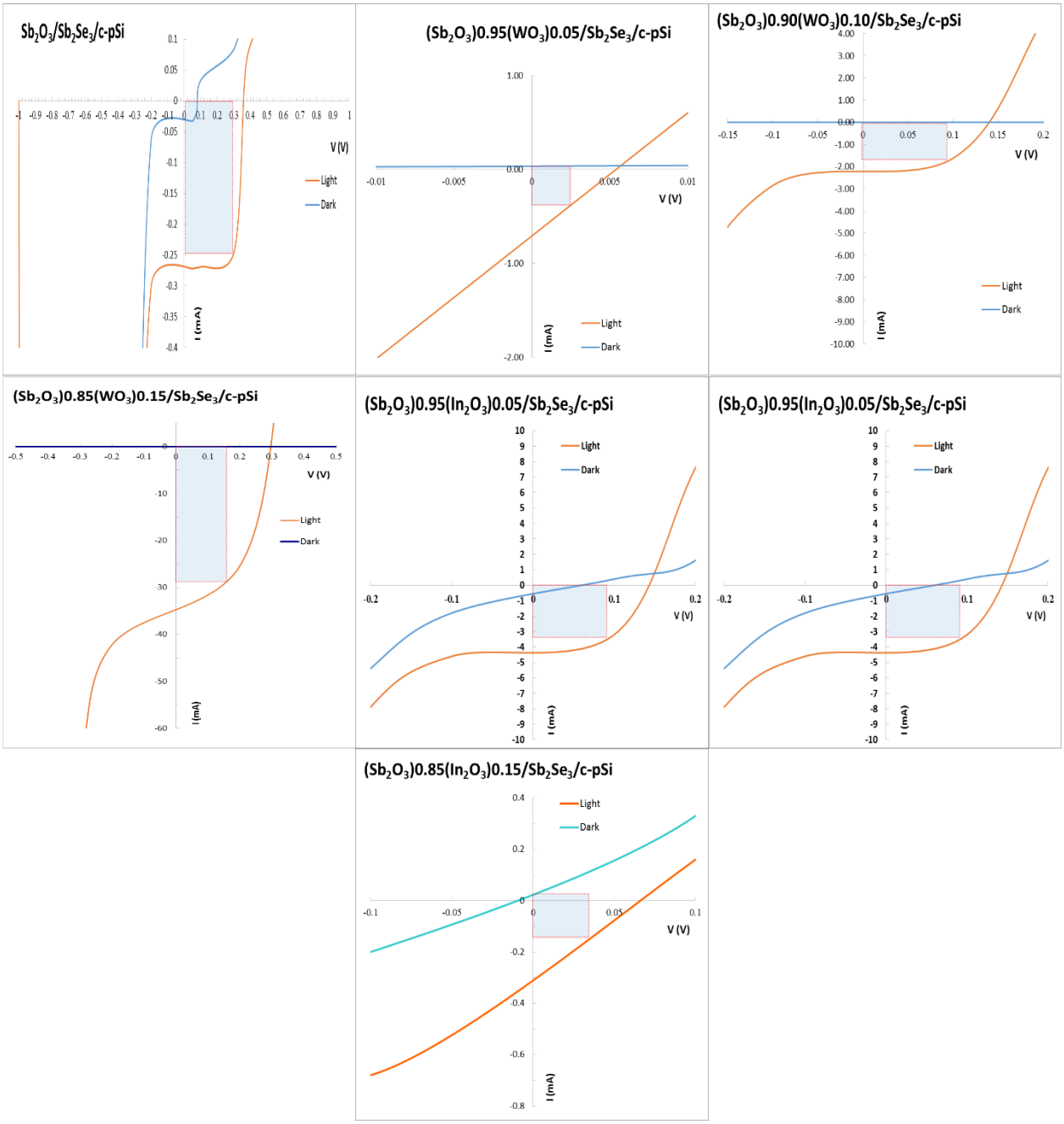

Figure 11: I-V characteristics of (Sb_2O_3:WO_3, In_2O_3 /Sb_2Se_3/c-pSi).

4. Conclusions

Heterojunction solar cells were fabricated from increasing tungsten oxide, which leads to a significant improvement in solar cell performance throughout increasing of conversion efficiency open circuit voltage and short circuit current while increasing indium oxide leads to performance enhancement of solar cell in the first but further addition leads to worsening the solar cell parameters.

Acknowledgements

The authors would like to thanks Department of Physics, College of science, University of Baghdad for supporting this work.

Conflict of Interest

Authors declare that they have no conflict of interest.

References

1. S. N. Esmaeel, J. Coll. Edu. **2**, 701 (2012).
2. K. Divya, P. Thomas, and K. Abraham, Mat. Sci. Semicon. Proce. **82**, 82 (2018).
3. A. J. Dennington, Ph.D Thesis, University of Bath, 2018.
4. W. K. Kadhim, J. Univ. Babylon Pu. Appl. Sci. **26**, 249 (2018).
5. A. Aracena, O. Jerez, and C. Antonucci, Transac. Nonfer. Met. Soci. China **26**, 294 (2016).
6. N. Tigau, Romanian J. Phys. **51**, 641 (2006).
7. F. Ding, Q. Wang, S. Zhou, G. Zhao, Y. Ye, and R. Ghomashchi, Roy. Soci. Op. Sci. **7**, 200479 (2020).
8. C. Song, N. Zhang, J. Lin, X. Guo, and X. Liu, Sci. Rep. **7**, 41250 (2017).
9. K. Divya and K. Abraham, Nano Expr. **1**, 020005 (2020).
10. Y. Shinde, P. Sonone, and A. Ubale, J. All. Comp. **831**, 154777 (2020).
11. M. Kamruzzaman, C. Liu, A. Farid Ul Islam, and J. Zapien, Semiconductors **51**, 1615 (2017).
12. Y. Abbas and A. A. Hasan, Iraqi J. Sci. **62**, 2915 (2021).
13. G. Franzò, A. Irrera, E. C. Moreira, M. Miritello, F. Iacona, D. Sanfilippo, G. Di Stefano, P. Fallica, and F. Priolo, Applied Physics A **74**, 1 (2002).
14. M. A. Abod, M.Sc. Thesis, University of Baghdad, (2022).
15. E. Voit, A. Panasenko, and L. Zemnukhova, J. Struc. Chem. **50**, 60 (2009).
16. S. Sen, A. Nilabh, and S. Kundu, Microchem. J. **165**, 106111 (2021).
17. J. Xu, B. Ma, L. Niu, C. Xu, Z. Chen, and Y. Lin, Adv. Compos. Lett. **28**, 0963693519865743 (2019).
18. E. J. U. D. S. D. N. F. I. Gallo, Ph.D Thesis, Universitá Degli Studi Di Napoli Federico II, 2009.
19. K. Chakarova, M. Mihaylov, and K. Hadjiivanov, Micropor. Mesopor. Mat. **345**, 112270 (2022).
20. R. J. Sáenz-Hernández, G. M. Herrera-Pérez, J. S. Uribe-Chavira, M. C. Grijalva-Castillo, J. T. Elizalde-Galindo, and J. A. Matutes-Aquino, Coatings **12**, 1727 (2022).
21. Y. Zhen, B. P. Jelle, and T. Gao, Analyt. Sci. Adv. **1**, 124 (2020).
22. S. H. Cho, K. M. Roccapriore, C. K. Dass, S. Ghosh, J. Choi, J. Noh, L. C. Reimnitz, S. Heo, K. Kim, and K. Xie, J. Chem. Phys. **152**, 014709 (2020).
23. M. Jothibas, C. Manoharan, S. Ramalingam, S. Dhanapandian, S. J. Jeyakumar, and M. Bououdina, J. Molec. Struc. **1049**, 239 (2013).
24. X. Zhao, Y. Zhou, D. Pan, Q. Liang, M. Zhou, S. Xu, Z. Li, and Y. Zhou, J. Envir. Chem. Eng. **11**, 109752 (2023).
25. X. Li, X. Wang, X. Ning, J. Lei, J. Shao, W. Wang, Y. Huang, and B. Hou, Appl. Surf. Sci. **462**, 155 (2018).
26. K. Ellmer, Charac. Mater., 564 (2012).
27. A. Pakdel, A. U. Khan, F. Pawula, S. Hébert, and T. Mori, Adv. Mat. Inter. **9**, 2200785 (2022).
28. Y.-C. Lin, Y.-K. Fei, and Y.-J. Hung, Sol. En. Mat. Sol. Cells **236**, 111520 (2022).
29. H. H. Abbas, M.Sc. Thesis, University of Baghdad, 2021.
30. S. Song, H. W. Cho, J. Jeong, Y. J. Yoon, S. Y. Park, S. Song, B. H. Woo, Y. C. Jun, B. Walker, and J. Y. Kim, Solar RRL **4**, 2000201 (2020).
31. H. R. Yeom, S. Song, S. Y. Park, H. S. Ryu, J. W. Kim, J. Heo, H. W. Cho, B. Walker, S.-J. Ko, and H. Y. Woo, Nano En. **77**, 105146 (2020).
32. Y. Singh, *Semiconductor devices* (New Delhi, India, IK International, 2013).
33. B. A. Hasan and H. H. Issa, Int. J. Adv. Sci. Tech. Res. **4**, 661.
34. A. A. Attia, F. S. Hashim, and K. H. Abass, Canadian J. Chem. **101**, 813 (2023).

35. V. Viswanathan, Ph.D Thesis, University of South Florida, 2004.
36. H. H. Issa and B. A. Hasan, Iraqi J. Phys. **13**, 42 (2015).
37. K. Walzer, B. Maennig, M. Pfeiffer, and K. Leo, Chem. Rev. **107**, 1233 (2007).
38. S. S. A. Shah, S. U. Awan, S. Zainab, H. Tariq, M. B. Riaz, A. Ul-Haq, N. Shahzad, and N. Iqbal, Opt. Mat. **141**, 113816 (2023).
39. M. A. Abood and B. A. Hasan, Iraqi J. Sci. **64**, 1675 (2023).
40. Z. Cao, W. Wang, J. Dong, L. Lou, H. Liu, Z. Wang, J. Luo, Y. Liu, Y. Dai, and D. Li, ACS Appl. Mat. Inter. **14**, 55691 (2022).
41. H. Shiel, T. D. Hobson, O. S. Hutter, L. J. Phillips, M. J. Smiles, L. A. Jones, T. J. Featherstone, J. E. Swallow, P. K. Thakur, and T.-L. Lee, J. Appl. Phys. **129**, 235301 (2021).
42. B. A. Hasan, Int. J. Adv. Res. Eng. Tech. **5**, 91 (2014).
43. B. A. Hasan, D. A. Umran, and M. a. K. Mankoshi, in Journal of Physics: Conference Series (IOP Publishing, 2018). p. 012020.
44. B. A. Hasan, Int. J. Adv. Sci. Tech. Res. **3**, 18 (2014).
45. B. A. Hasan and H. H. Issa, Int. J. Adv. Sci. Tech. Res. **3**, 661 (2014).
46. S. Sengupta, R. Aggarwal, and M. Raula, J. Mat. Res. **38**, 142 (2023).
47. R. Kondrotas, C. Chen, and J. Tang, Joule **2**, 857 (2018).
48. M. A. Abood and B. A. Hasan, Iraqi J. Sci. **64**, 2282 (2023).
49. H. H. Abass and B. A. Hasan, Iraqi J. Phys. **19**, 41 (2021).
50. B. A. Hasan, in IOP Conference Series: Materials Science and Engineering (IOP Publishing, 2020). p. 072011.

التوصيف والتأثير الكهروضوئي للمفارق الغير متجانسة (Sb_2O_3: اكاسيد المعادن) /*C-Si*

محمد عماد طارق[1] وبشرى عباس حسن[1]
[1] قسم الفيزياء، كلية العلوم، جامعة بغداد، بغداد، العراق

الخلاصة

في هذا العمل تم تحضير نوعين من المتراكبات من أوكسيد الانتمون مع اوكسيد التنكستن واوكسيد الانتمون مع اوكسيد الانديوم تم تحضيرها كأغشية رقيقة من (Sb_2O_3):(WO_3,In_2O_3) باستخدام الترسيب بالليزر النبضي ، باستخدام تحويلات فورير اكد وجود اوكسيد الانتمون, اوكسيد التنكستن واوكسيد الانديوم, اظهر قياس تأثير هول ان الاغشية الرقيقة النانوية لأوكسيد الانتيمون من النوع p يتم تحولها تدريجيا الى النوع n بإضافة اكسيد التنكستن بينما يتم تحوليا انيا الى النوع n بإضافة اوكسيد الانديوم. تم تحضير مفارق هجينة من (Sb_2O_3:WO_3,In_2O3//Sb_2Se_3/c-pSi) والتي تتألف من طبقتين الاولى Sb_2Se_3 والثانية هي الاغشية النانوية من (Sb_2O_3:WO_3,In_2O_3/c-pSi). اظهرت المفارق الهجينة المحضرة أفضل كفاءة 9% وفولتية دائرة مفتوحة 300 mV وتيار دائرة قصيرة35 mA عند شدة اضاءة 100 mW/cm^2.

الكلمات المفتاحية: الخلايا الشمسية، الترسيب بالليزر النبضي، اغشية Sb_2O_3 الرقيقة، طيف FTIR, تأثير هول.